











Cite this: DOI: 10.1039/c8nr05241g

## Ultrastretchable carbon nanotube composite electrodes for flexible lithium-ion batteries†

Yang Yu, <sup>a,b</sup> Yufeng Luo, <sup>a,b</sup> Hengcai Wu, <sup>a</sup> Kaili Jiang, <sup>a,c</sup> Qunqing Li, <sup>a,c</sup> Shoushan Fan, <sup>a,b</sup> Ju Li \*<sup>d</sup> and Jiaping Wang \*<sup>a,c,d</sup>

Ultra-stretchable carbon nanotube (CNT) composite electrodes for lithium-ion batteries are fabricated by coating CNT films and active material powders on biaxially pre-strained polydimethylsiloxane (PDMS) substrates. The wrinkled structures that form during the pre-straining and release process extend along the strain axis to protect the CNT composite structures from fracture. The CNT composites demonstrate excellent stability and high durability with resistance increase of less than 12% after 2000 cycles at 150% strain. Both CNT/Li<sub>4</sub>Ti<sub>5</sub>O<sub>12</sub> (LTO) anodes and CNT/Li(Ni<sub>1/3</sub>Co<sub>1/3</sub>Mn<sub>1/3</sub>)O<sub>2</sub> (NCM) cathodes maintain excellent electrochemical properties at cyclic 150% strain in different axes. The full lithium-ion battery consisting of the stretchable CNT/LTO anode and CNT/NCM cathode is able to withstand 150% strain in different axes without large decreases in performance. Stretchable batteries fabricated by the scalable, highly efficient, and low-cost biaxial pre-strain process with excellent durability and electrochemical properties will have potential applications in flexible devices.

Received 29th June 2018,  
Accepted 16th October 2018

DOI: 10.1039/c8nr05241g

rsc.li/nanoscale

### 1. Introduction

The growth of implantable and epidermal devices has promoted the rapid development of high-performance flexible and stretchable electronic devices.<sup>1–7</sup> The implantable or epidermal devices need to be not only flexible but also stretchable to match the properties of soft and elastic biological tissue. Many high-performance stretchable electronic devices, including strain or temperature sensors,<sup>8–11</sup> displays,<sup>12–14</sup> and cameras,<sup>15,16</sup> have been designed. As a result, a critical need lies in energy-storage devices with similar physical properties to maximize the stretchability of these devices. Different kinds of energy-storage devices that can work well while being stretched have been developed, such as alkaline batteries,<sup>17</sup> solar cells,<sup>18</sup> and supercapacitors.<sup>19–21</sup> Owing to the combination of high voltage, large energy density, and long life, lithium-ion batteries (LIBs) are perceived to have the most potential for application as energy storage systems to power stretchable devices.<sup>22–24</sup> Many attempts have been made to fab-

ricate LIBs that can withstand strain, and many structures have been designed to achieve stretchable LIBs, including serpentine interconnections,<sup>25</sup> origami structures,<sup>26,27</sup> and spring fibers.<sup>28</sup> For example, rigid battery cells that were distributed as islands were connected by serpentine metal conductors and could withstand approximately 300% strain along different axes without failure.<sup>25</sup> However, the structure had poor tensile durability at this high strain level.

Recently, buckled structures formed on the surface of non-stretchable films were used to design stretchable electronics.<sup>29–31</sup> As these structures were able to flatten to endure deformation during stretching, semiconductor nanoribbons,<sup>29</sup> conductors<sup>21</sup> and other devices<sup>31</sup> with buckled structures could stand high and repeated tensile loading. Carbon nanomaterials, such as carbon nanotubes (CNTs) and graphene, are considered as promising materials for developing high performance lithium batteries because of their high surface area, mechanical robustness and excellent electrical conductivity.<sup>32–36</sup> By combining buckled structures and carbon nanomaterials, stretchable energy-storage devices with wavy configurations were fabricated, including supercapacitors<sup>19,21,37</sup> and batteries.<sup>38</sup> Stretchable batteries based on arched CNT structures could withstand repeated 400% strain, but only in one direction.<sup>38</sup> Therefore, there is an urgent need to develop high-performance stretchable batteries that can withstand large and repeated tensile cycles in different axes.

Super-aligned CNTs have attracted much attention in recent years.<sup>39</sup> Cost-effective, ultrathin, and continuous CNT films

<sup>a</sup>Department of Physics and Tsinghua-Foxconn Nanotechnology Research Center, Tsinghua University, Beijing, China. E-mail: jpwang@tsinghua.edu.cn

<sup>b</sup>School of Materials Science and Engineering, Tsinghua University, Beijing, China

<sup>c</sup>Collaborative Innovation Center of Quantum Matter, Beijing, China

<sup>d</sup>Department of Nuclear Science and Engineering and Department of Materials Science and Engineering, Massachusetts Institute of Technology, Cambridge, MA 02139, USA. E-mail: liju@mit.edu

† Electronic supplementary information (ESI) available. See DOI: 10.1039/c8nr05241g

can be drawn from super-aligned CNT arrays by an end-to-end joining mechanism and stacked together.<sup>40</sup> Freestanding, lightweight CNT films possess excellent electrical and mechanical properties and have demonstrated applications in loudspeakers,<sup>41</sup> touch screens,<sup>39</sup> and conductors.<sup>42</sup> The thickness of the CNT films depends on the number of CNT layers. By compositing the films with other materials, CNT films have been widely used for the development of high-performance electrodes for LIBs<sup>43–48</sup> and other energy storage devices.<sup>49</sup>

In this work, ultra-stretchable CNT composite electrodes were fabricated by coating CNT films and active material powders on biaxially pre-strained polydimethylsiloxane (PDMS) substrates. These electrodes could withstand high and repeated strain in different axes. Wrinkled structures that formed during the pre-straining and release process extended along the strain axis to protect the CNT composite structures from fracture. The CNT composite electrodes maintained excellent electrochemical properties after 2000 tensile cycles at 0–150% strain in different axes. Full LIBs with stretchable electrodes were able to withstand 150% strain in different axes without a significant decrease in their properties. These stretchable batteries with excellent durability and electrochemical properties will have potential applications in flexible devices.

## 2. Results and discussion

### 2.1 Fabrication and resistance changes of the CNT composite electrodes

A schematic representation of the fabrication process of the stretchable CNT composite electrodes is shown in Fig. 1a. First, a PDMS square substrate with a length  $L$  was biaxially pre-strained in two perpendicular directions to  $L + \Delta L$ , and

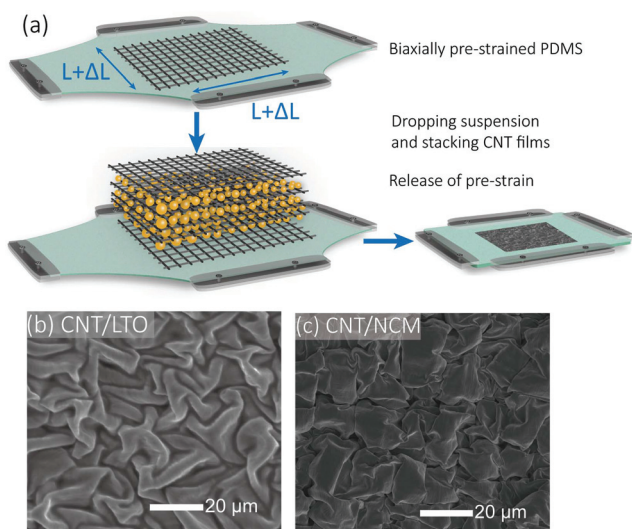


**Fig. 1** (a) Schematic of the process for fabricating stretchable CNT electrodes; SEM images of the (a) CNT/LTO and (b) CNT/NCM electrodes.

then coated with a cross-stacked 6-layer CNT film. Then, suspensions of  $\text{Li}(\text{Ni}_{1/3}\text{Co}_{1/3}\text{Mn}_{1/3})\text{O}_2$  (NCM, Kejing Star Technology Co., Shenzhen, China) or  $\text{Li}_4\text{Ti}_5\text{O}_{12}$  (LTO, Reshine, China) powder in ethanol were dropped on the CNT film with a pipette, followed by cross-stacking a 2-layer CNT film. After the evaporation of ethanol, the dropping of the suspension and stacking of the CNT film were repeated 10 times. Finally, another cross-stacked 6-layer CNT film was placed on the top to form a sandwiched structure. The active materials were fully covered and entrapped by the CNT network and a continuous buckled composite electrode was formed on the surface of the PDMS substrate. The interfacial adhesion between the PDMS surface and the CNT film was very strong due to the clean surface of CNTs and the large van der Waals force. Without using any binder, the buckled CNT film on the surface of the PDMS demonstrated structural stability after 10 000 tensile cycles at 150% strain as reported in our previous paper.<sup>50</sup> After the pre-strained PDMS substrate was released to its original length  $L$ , CNT composite electrodes were fabricated. The areal densities of both NCM and LTO are  $5 \text{ mg cm}^{-2}$ , accounting for about 95 wt% in the composite electrodes. Fig. S2† shows the XRD patterns of the NCM and LTO powders and the NCM/CNT and LTO/CNT electrodes. Characteristic diffraction peaks of NCM and LTO were observed in both pure powders and composite electrodes. In the NCM/CNT and LTO/CNT electrodes, diffraction peak of CNT did not appear due to its limited content. Fig. 1b and c show the SEM images of the CNT/LTO and CNT/NCM composite electrodes; wrinkled structures were observed on the surface of the composite electrodes.

The normalized resistance changes ( $\Delta R/R_0$ ) of the CNT/LTO and CNT/NCM electrodes as a function of the applied strain in different axes ( $X$ ,  $Y$ , and  $45^\circ$ ) are shown in Fig. 2a and b. The

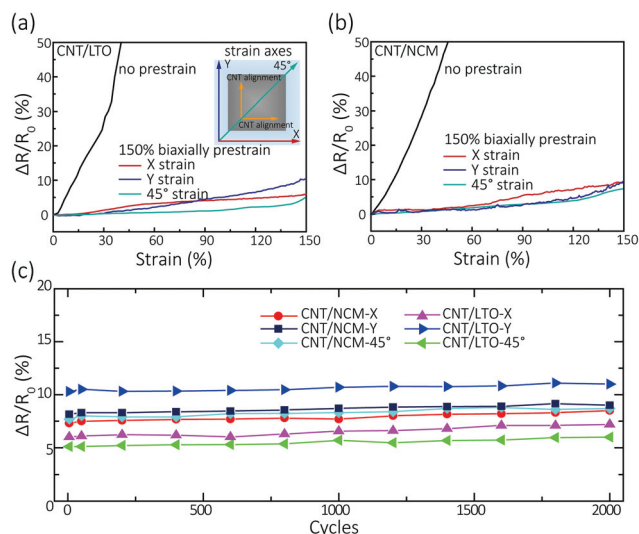


**Fig. 2** Normalized resistance changes of the (a) CNT/LTO and (b) CNT/NCM electrodes as a function of applied strain in different axes. Inset shows the strain axes. (c) Normalized resistance changes of the pre-strained CNT/LTO and CNT/NCM electrodes during 2000 cycles at 0–150% strain in different axes.

strain axes are shown in the inset of Fig. 2a. The *X* and *Y* strain axes are parallel to the alignment of the CNTs. The CNT/LTO electrode without pre-strain showed a sharp increase in resistance as the applied strain increased. The normalized resistance increased by 50% at 40% strain in the *X* axis. Such an increase in resistance would obviously impair the electrochemical performance of the electrode. For the CNT/LTO electrode with a 150% biaxial pre-strain, the normalized resistance change was more stable at an applied strain of 150% in different tensile axes, with increases of 6%, 10.6%, and 5% at 150% strain in the *X*, *Y*, and 45° axes, respectively (Fig. 2a). Similar resistance changes as a function of the applied strain were observed in the biaxially pre-stained CNT/NCM electrode. Without pre-straining, the normalized resistance of the CNT/NCM electrode increased by 50% at 50% strain in the *X* axis. The normalized resistance of the CNT/NCM electrode with biaxial pre-strain increased only 8.9%, 9.6%, and 7.2% at 150% strain in the *X*, *Y*, and 45° axes (Fig. 2b).

To characterize the stretchability of the CNT electrodes, they were cycled between 0 and 150% strain in different axes (*X*, *Y*, and 45°) and the resistances were monitored after each cycle. The normalized resistance changes of the biaxially pre-stained CNT/LTO and CNT/NCM electrodes during 2000 tensile cycles are shown in Fig. 2c. The normalized resistances of the CNT composite electrodes showed less than 12% increase at strains along all the axes in the cyclic tensile test. The normalized resistance of the CNT/LTO electrode only increased 2.1% after 2000 tensile cycles at 0–150% strain in the 45° axis. The constant resistance of the CNT/LTO and CNT/NCM electrodes suggests that the CNT conductive structures did not fracture during the cyclic tensile testing in different axes.

The SEM images in Fig. 3 show the surface morphologies of the CNT/LTO electrode at strain in different axes. Disordered wrinkled structures that formed during the biaxial pre-straining process were observed on the surface (Fig. 3(a)). When 150% strain in the *Y* axis was applied to the sample, the wrinkled structures extended along the strain axis, as shown in

Fig. 3(b). The wavy structures were parallel to the applied strain axis, which were formed due to the compression of the CNT/LTO electrode in the direction perpendicular to the strain axis. The conductive network in the electrode remained intact at 150% strain without obvious fracture of the CNT film, resulting in a constant resistance of the electrodes during the tensile process (Fig. 2a). Similarly, when the strain was applied in the *X* and 45° axes, the wrinkled structures that formed during the biaxial pre-straining process extended along the strain axes to remain a continuous and conductive network in the electrode, as shown in Fig. 3(c) and (d). In particular, the wrinkled structures became flat when strains were applied in both *X* and *Y* axes at the same time, as shown in Fig. 3(e). The CNT/LTO electrode remained intact when strains were applied in both *X* and *Y* axes, showing its stretchability in two directions. Moreover, the extensions of the wrinkled structures at strain in different axes were reversible. When the 150% strain in the *Y* axis was released, the wavy structures fully converted to the initially disordered wrinkled structures, as shown in Fig. 3(f).

The morphologies of the CNT/LTO electrode with 150% biaxial pre-strain before and after cyclic tensile test in the *X* axis are shown in Fig. 4. The wrinkled structures on the surface extended and recovered with the loading and release of the strain. No structural failure was present in the biaxially pre-stained CNT/LTO electrode after 2000 tensile cycles at 0–150% strain. Similar phenomena were observed in the CNT/NCM electrode before and after tensile cycles at 0–150% strain in the *X* axis (Fig. S1†). The continuous and conductive CNT network in the composite electrodes remained intact after the cyclic tensile test because of the excellent mechanical properties of the CNT film and the reversible extension of the wrinkled structures, which resulted in stable resistances of the CNT/LTO and CNT/NCM electrodes during the 2000 tensile cycles at strain in the *X*, *Y*, and 45° axes, as shown in Fig. 2c. These results indicate that stretchable CNT composite electrodes can be fabricated using the biaxial prestrain process with almost constant resistance during long-term tensile cycles in different axes, which is of great value for use in high-performance stretchable batteries.

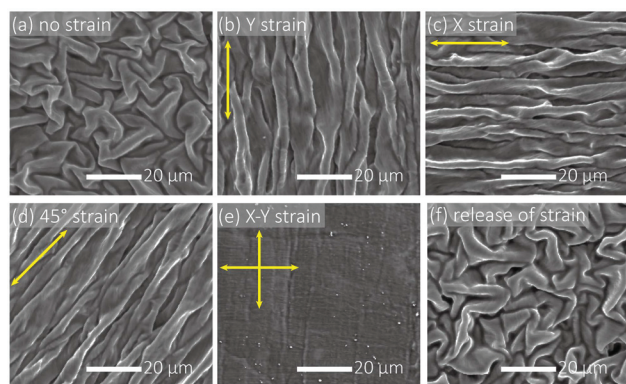


**Fig. 3** SEM images of the CNT/LTO electrode: (a) at zero strain; morphology evolution at 150% strain in the (b) *Y*, (c) *X*, (d) 45°, (e) *X* and *Y* axes; and (f) after release of strain.

## 2.2 Electrochemical properties of CNT composite electrodes

The electrochemical properties of the stretchable CNT/LTO anode were characterized using half-cells with lithium foil as

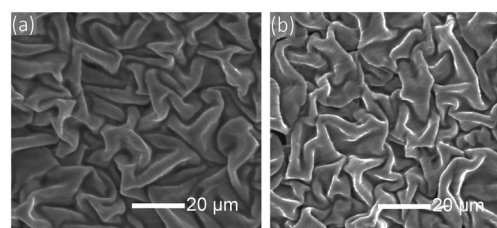


**Fig. 4** SEM images of the CNT/LTO electrode (a) before and (b) after 2000 tensile cycles at 0–150% strain in the *X* axis.



the counter electrode. Galvanostatic tests were carried out in a voltage window of 1.0–2.5 V *versus* Li/Li<sup>+</sup>. The cycling performances of the CNT/LTO anode at zero strain and at 150% strain in different axes at a current density of 0.1C are shown in Fig. 5a. The biaxially pre-strained CNT/LTO anode presented excellent cycling performance. At zero strain, the initial specific capacity was 150 mA h g<sup>-1</sup>, which is the same level as other CNT/LTO anodes reported in the literature.<sup>38,51,52</sup> It delivered a specific capacity of 146 mA h g<sup>-1</sup> after 100 cycles, corresponding to a capacity retention of 97.3%, indicating excellent reversibility. Strains as high as 150% in different axes had little effect on the cycling performance of the biaxially pre-strained CNT/LTO anodes. The initial specific capacities slightly decreased to 149, 147, and 148 mA h g<sup>-1</sup> when 150% strains were loaded in the X, Y, and 45° axes. After 100 cycles at 0.1C, the reversible capacities of the stretchable anode at 150% strains were still as high as 140 (X axis), 138 (Y axis), and 143 (45° axis) mA h g<sup>-1</sup>, corresponding to capacity retentions of 93.9%, 93.8%, and 96.9%. The CNT/LTO electrode at strain in the 45° axis exhibited the highest specific capacity and retention rate.

CNT/LTO electrodes with different areal densities of LTO were characterized at zero strain and at 150% strain. As shown in Fig. S3,† at zero strain, the initial specific capacity of the CNT/LTO electrode remained stable at around 150 mA h g<sup>-1</sup> with areal density of LTO below 5 mg cm<sup>-2</sup>. It gradually decreased to 120 mA h g<sup>-1</sup> as the areal density increased to 10 mg cm<sup>-2</sup>. At 150% strain, the initial specific capacity also maintained stable but decreased quickly when the areal density of LTO became larger than 5 mg cm<sup>-2</sup>. As the areal density of LTO increased, the specific contact area between the LTO powders and the CNT film decreased, and both stretchability and conductivity of the CNT/LTO electrode were degraded, resulting in the decrease of the specific capacity.

Samples with an areal density of LTO at 5 mg cm<sup>-2</sup> demonstrated a combination of high energy density and excellent stretchability, thus are more suitable for developing stretchable energy devices. The experiments and analyses below are all based on samples with an areal density of active electrode material at 5 mg cm<sup>-2</sup>.

The rate performances of the CNT/LTO anode were characterized at a constant discharge rate of 0.1C and varied charge rates (Fig. 5b). At zero strain, the reversible capacities reached 148, 146, 145, 144, 143, and 142 mA h g<sup>-1</sup> at charge current densities of 0.1C, 0.2C, 0.5C, 1C, 2C, and 5C, respectively, which are much higher than those of the stretchable anodes reported in the literature.<sup>30</sup> The good rate performance of the CNT/LTO anodes is ascribed to the efficient electron and ion transfers in the sandwich structured electrodes and the excellent mechanical properties of the CNT network.<sup>42</sup> When the discharge current density was reverted to 0.1C, the CNT/LTO electrode delivered a specific capacity of 146 mA h g<sup>-1</sup>, indicating excellent reversibility of the electrode. The CNT/LTO electrodes were able to maintain excellent rate performances when 150% strain was applied in different axes. The specific capacities of the CNT/LTO electrode at 5C were 137, 136, and 139 mA h g<sup>-1</sup> at 150% strains in the X, Y, and 45° axes, with high capacity retentions of 91.9%, 93.2%, and 94.2%, respectively, compared with their value at 0.1C. Because the wrinkled structures extended along the strain axes to protect the CNT conductive network from fracture, the CNT/LTO anodes retained remarkable cycle and rate performances at 150% strains in different axes.

To demonstrate the electrochemical properties of the CNT composite electrodes after repeated tensile cycles, the dependence of the electrochemical stability of the CNT/LTO anode on the number of tensile cycles was investigated (Fig. 5c). Only a slight capacity decay was observed during the tensile cycles. The capacity retentions of the CNT/LTO anode after 2000 tensile cycles at 0–150% strain in the X, Y, and 45° axes were 92.7%, 91.3%, and 96.0%, respectively. The charge–discharge curves of the CNT/LTO anode after 2000 tensile cycles at 0–150% strain in the X, Y, and 45° axes at 0.1C are shown in Fig. 5d. The charge–discharge curves almost coincide with the curves before the tensile cycles. The specific capacities after 2000 tensile cycles at 0–150% strain in the X, Y, and 45° axes were 140, 137, and 145 mA h g<sup>-1</sup>, respectively. The cyclic tensile strain had little effect on the charge/discharge processes of the CNT/LTO electrode, demonstrating its excellent strain durability.

The CNT/NCM electrodes also possessed excellent electrochemical properties at high and repeated strains. At zero strain, it showed an initial specific capacity of 147 mA h g<sup>-1</sup> at 0.1C with a capacity retention of 97.3% after 100 charge–discharge cycles (Fig. S4†). As the charge current increased to 5C, its specific capacity decreased to 132 mA h g<sup>-1</sup>. At 150% strain in different axes, the specific capacities of the CNT/NCM electrode were still higher than 144 mA h g<sup>-1</sup> at 0.1C and 128 mA h g<sup>-1</sup> at 5C (Fig. S4a and b†). After 2000 tensile cycles at 0–150% strain in different axes, it delivered a reversible

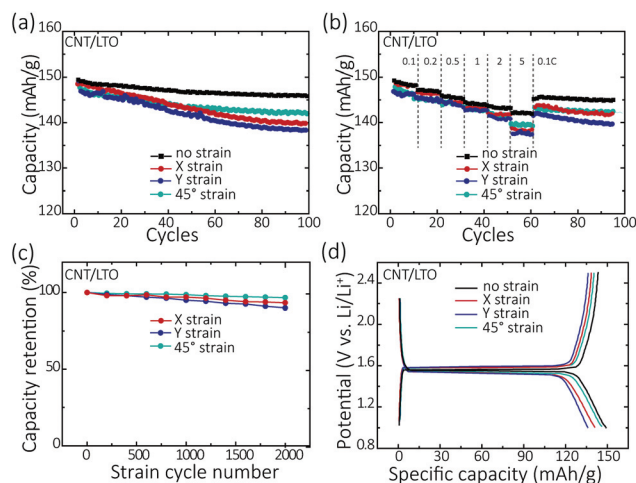


**Fig. 5** (a) Cycling and (b) rate performances of the CNT/LTO electrodes at zero strain and at 150% strain in different axes; (c) capacity retention and (d) voltage profiles of the CNT/LTO electrode after 2000 tensile cycles at 0–150% strain in different axes.

capacity of  $134 \text{ mA h g}^{-1}$  (Fig. S4c and d†). The high electrochemical stability of both CNT/LTO and CNT/NCM electrodes during the 2000 tensile cycles at 0–150% strain demonstrated that they were able to maintain stable structures at high and cyclic strain conditions, due to the reversible extension of the wrinkled structures that formed during the biaxial pre-strain process.

### 2.3 Electrochemical properties of the stretchable full batteries

Ultra-stretchable full batteries with CNT/LTO anodes, CNT/NCM cathodes, and gel electrolyte were assembled, as schematically shown in Fig. 6. The gel electrolyte was prepared by dissolving poly (ethylene oxide) (PEO), succinonitrile, and lithium bis(trifluoromethane) sulfonimide (LiTFSi) in mixed solvent of methylene chloride and acetone. The thickness of the gel electrolyte is about 0.6 mm. The full batteries were cycled at 0.1C in a voltage window of 1.6–2.8 V. At zero strain, the initial specific capacity of the full battery was  $0.52 \text{ mA h cm}^{-2}$  (Fig. 7a). After 50 charge–discharge cycles, it delivered a reversible capacity of  $0.47 \text{ mA h cm}^{-2}$ , showing a capacity retention of 90.3%. At 150% strain in the X, Y, and  $45^\circ$  axes, the initial specific capacities were almost unchanged and delivered reversible capacities of 0.41, 0.37, and  $0.40 \text{ mA h cm}^{-2}$  respectively after 50 charge–discharge cycles. The electrochemical properties of stretchable full batteries can be affected by many factors such as the deformation of the gel electrolyte. Capacity retention rates were similar for full NCM/LTO batteries at strains in the X, Y, and  $45^\circ$  axes, compared to the highest capacity and retention rate in the  $45^\circ$  axes for the CNT/LTO electrode. The high capacity retentions at strain in different axes demonstrated the ultra-stretchability of the full batteries.

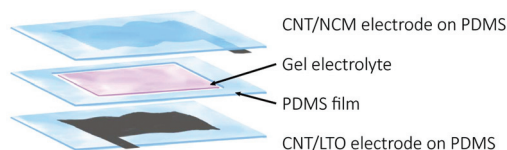


Fig. 6 Schematic illustration of the structure of a stretchable full battery.

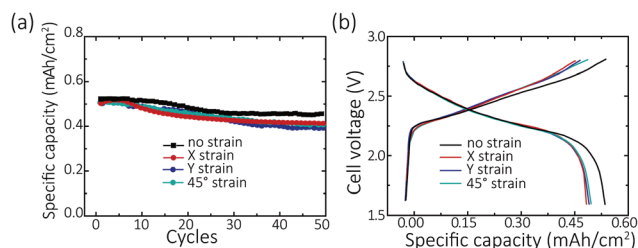


Fig. 7 (a) Cycling performances of the full NCM/LTO battery at 0.1C at zero strain and at 150% strain in different axes. (b) Voltage profiles of the full NCM/LTO battery after 2000 tensile cycles at 0–150% strain in different axes.

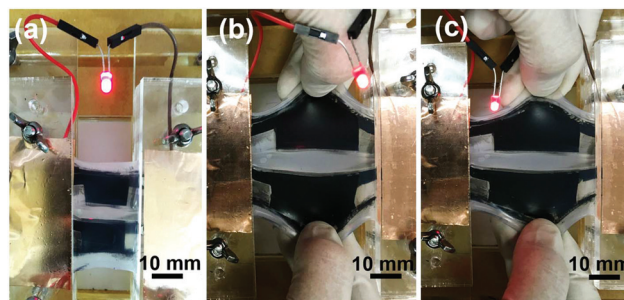


Fig. 8 An illuminated LED powered by stretchable NCM/LTO batteries (a) at zero strain, (b) at strain in both X and Y axes, and (c) after 50 strain cycles.

The ultra-stretchable full batteries also had excellent durability. The voltage profiles of the full battery after 2000 tensile cycles at 0–150% strain in the X, Y, and  $45^\circ$  axes are shown in Fig. 7b. Its reversible capacities were still as high as 0.47, 0.49, and  $0.50 \text{ mA h cm}^{-2}$ , respectively, after 2000 tensile cycles at strain in the X, Y, and  $45^\circ$  axes, demonstrating excellent durability of the full battery. The high durability is attributed to the highly reversible morphological changes of both CNT/LTO and CNT/NCM electrodes during the tensile cycles and the excellent mechanical properties of the CNT films. Therefore, full batteries based on the CNT composite electrodes could withstand strain as high as 150% in different axes without any evident decay in their electrochemical properties and presented stable electrochemical performance after 2000 tensile cycles at 0–150% strain in different axes.

Finally, to directly demonstrate the stretchability of the full batteries, an LED was illuminated by two parallel full CNT/LTO-CNT/NCM batteries, as shown in Fig. 8a. The LED did not show any noticeable luminance fluctuation when the batteries were stretched approximately 100% in both X and Y axes at the same time (Fig. 8b), even after 50 strain cycles (Fig. 8c). These results demonstrated that the stretchable batteries were able to withstand high cyclic strain in different axes and held great potential for use in stretchable electronic devices.

## 3. Conclusions

Ultra-stretchable CNT composite electrodes were fabricated by stacking CNT films and LTO or NCM powders on biaxially pre-stretched PDMS substrates and forming disordered wrinkled structures after the release of the pre-strain. The wrinkled structures accommodated large strains in different axes to protect the CNT composites from fracture, resulting in their high stretchability and durability. Both CNT/LTO and CNT/NCM electrodes had excellent electrochemical properties and were able to withstand high and repeated strain (0–150%) in different axes without significant performance decay. The full batteries consisting of CNT/LTO anodes and CNT/NCM cathodes also maintained stable electrochemical performances at

150% strain in different axes. In addition, the fabrication process is scalable owing to the use of commercial electrode materials and the highly efficient and low-cost pre-strain process. This biaxial pre-strain process presents an effective route in developing ultra-stretchable electronic devices, including photovoltaic devices and other energy storage devices.

## Conflicts of interest

There are no conflicts to declare.

## Acknowledgements

JW acknowledges support by NSFC-51472141. QL acknowledges support by National Key Research and Development Program of China-2017YFA0205800. JL acknowledges support by NSF ECCS-1610806.

## Notes and references

- J. A. Rogers, T. Someya and Y. G. Huang, *Science*, 2010, **327**, 1603–1607.
- J. Kim, G. A. Salvatore, H. Araki, A. M. Chiarelli, Z. Xie, A. Banks, X. Sheng, Y. Liu, J. W. Lee, K.-I. Jang, S. Y. Heo, K. Cho, H. Luo, B. Zimmerman, J. Kim, L. Yan, X. Feng, S. Xu, M. Fabiani, G. Gratton, Y. Huang, U. Paik and J. A. Rogers, *Sci. Adv.*, 2016, **2**, 1600418.
- B. Y. Ahn, E. B. Duoss, M. J. Motala, X. Guo, S.-I. Park, Y. Xiong, J. Yoon, R. G. Nuzzo, J. A. Rogers and J. A. Lewis, *Science*, 2009, **323**, 1590–1593.
- D. Y. Khang, H. Q. Jiang, Y. Huang and J. A. Rogers, *Science*, 2006, **311**, 208–212.
- D.-H. Kim, J.-H. Ahn, W. M. Choi, H.-S. Kim, T.-H. Kim, J. Song, Y. Y. Huang, Z. Liu, C. Lu and J. A. Rogers, *Science*, 2008, **320**, 507–511.
- K. S. Kim, Y. Zhao, H. Jang, S. Y. Lee, J. M. Kim, K. S. Kim, J.-H. Ahn, P. Kim, J.-Y. Choi and B. H. Hong, *Nature*, 2009, **457**, 706–710.
- J.-Y. Sun, X. Zhao, W. R. K. Illeperuma, O. Chaudhuri, K. H. Oh, D. J. Mooney, J. J. Vlassak and Z. Suo, *Nature*, 2012, **489**, 133–136.
- D. J. Lipomi, M. Vosgueritchian, B. C. K. Tee, S. L. Hellstrom, J. A. Lee, C. H. Fox and Z. Bao, *Nat. Nanotechnol.*, 2011, **6**, 788–792.
- S. C. B. Mannsfeld, B. C. K. Tee, R. M. Stoltenberg, C. V. H. Chen, S. Barman, B. V. O. Muir, A. N. Sokolov, C. Reese and Z. Bao, *Nat. Mater.*, 2010, **9**, 859–864.
- T. Yamada, Y. Hayamizu, Y. Yamamoto, Y. Yomogida, A. Izadi-Najafabadi, D. N. Futaba and K. Hata, *Nat. Nanotechnol.*, 2011, **6**, 296–301.
- L. Tian, Y. Li, R. C. Webb, S. Krishnan, Z. Bian, J. Song, X. Ning, K. Crawford, J. Kurniawan, A. Bonifas, J. Ma, Y. Liu, X. Xie, J. Chen, Y. Liu, Z. Shi, T. Wu, R. Ning, D. Li, S. Sinha, D. G. Cahill, Y. Huang and J. A. Rogers, *Adv. Funct. Mater.*, 2017, **27**, 1701282.
- L. Donaldson, *Mater. Today*, 2013, **16**, 416–416.
- H. B. Wang, S. Z. D. Cheng and F. W. Harris, *Abstr. Pap. Am. Chem. Soc.*, 2001, **221**, U308–U308.
- H. Yongtaek, L. Byeongmoon, O. Eunho and B. Junghwan, *Inf. Disp.*, 2017, **33**, 6–11.
- Z. Li and J. Xiao, *J. Appl. Phys.*, 2015, **117**, 014904.
- J. A. Rogers, *Science*, 2009, **327**, 1603–1607.
- A. M. Gaikwad, A. M. Zamarayeva, J. Rousseau, H. Chu, I. Derin and D. A. Steingart, *Adv. Mater.*, 2012, **24**, 5071–5076.
- J. Lee, J. Wu, M. Shi, J. Yoon, S.-I. Park, M. Li, Z. Liu, Y. Huang and J. A. Rogers, *Adv. Mater.*, 2011, **23**, 986–991.
- J. Zang, C. Cao, Y. Feng, J. Liu and X. Zhao, *Sci. Rep.*, 2014, **4**, 6492.
- K. H. An, W. S. Kim, Y. S. Park, Y. C. Choi, S. M. Lee, D. C. Chung, D. J. Bae, S. C. Lim and Y. H. Lee, *Adv. Mater.*, 2001, **13**, 497.
- C. Yu, C. Masarapu, J. Rong, B. Wei and H. Jiang, *Adv. Mater.*, 2009, **21**, 4793.
- N.-S. Choi, Z. Chen, S. A. Freunberger, X. Ji, Y.-K. Sun, K. Amine, G. Yushin, L. F. Nazar, J. Cho and P. G. Bruce, *Angew. Chem., Int. Ed.*, 2012, **51**, 9994–10024.
- V. Etacheri, R. Marom, R. Elazari, G. Salitra and D. Aurbach, *Energy Environ. Sci.*, 2011, **4**, 3243–3262.
- Y. Gogotsi and P. Simon, *Science*, 2011, **334**, 917–918.
- S. Xu, Y. Zhang, J. Cho, J. Lee, X. Huang, L. Jia, J. A. Fan, Y. Su, J. Su, H. Zhang, H. Cheng, B. Lu, C. Yu, C. Chuang, T.-I. Kim, T. Song, K. Shigeta, S. Kang, C. Dagdeviren, I. Petrov, P. V. Braun, Y. Huang, U. Paik and J. A. Rogers, *Nat. Commun.*, 2013, **4**, 1543.
- S.-J. Cho, K.-H. Choi, J.-T. Yoo, J.-H. Kim, Y.-H. Lee, S.-J. Chun, S.-B. Park, D.-H. Choi, Q. Wu, S.-Y. Lee and S.-Y. Lee, *Adv. Funct. Mater.*, 2015, **25**, 6029–6040.
- Z. Song, T. Ma, R. Tang, Q. Cheng, X. Wang, D. Krishnaraju, R. Panat, C. K. Chan, H. Yu and H. Jiang, *Nat. Commun.*, 2014, **5**, 3140.
- Y. Zhang, W. Bai, X. Cheng, J. Ren, W. Weng, P. Chen, X. Fang, Z. Zhang and H. Peng, *Angew. Chem., Int. Ed.*, 2014, **53**, 14564–14568.
- Y. Sun, W. M. Choi, H. Jiang, Y. Y. Huang and J. A. Rogers, *Nat. Nanotechnol.*, 2006, **1**, 201–207.
- T. W. Ebbesen and P. M. Ajayan, *Nature*, 1992, **358**, 220–222.
- J. Kim, M. Lee, H. J. Shim, R. Ghaffari, H. R. Cho, D. Son, Y. H. Jung, M. Soh, C. Choi, S. Jung, K. Chu, D. Jeon, S.-T. Lee, J. H. Kim, S. H. Choi, T. Hyeon and D.-H. Kim, *Nat. Commun.*, 2014, **5**, 5747.
- J. KaiLi, W. JiaPing, L. I. QunQing, L. I. U. Liang, L. I. U. ChangHong and F. A. N. ShouShan, *Sci. Sin. Phys., Mech. Astron.*, 2011, **41**, 390–403.
- P. Avouris, J. Appenzeller, V. Derycke, R. Martel and S. Wind and I. Electronic Devices Society Of Ieee, Electronic Devices Society Of, *Carbon nanotube electronics*, 2002.
- S. W. Lee, N. Yabuuchi, B. M. Gallant, S. Chen, B. Kim, P. T. Hammond and Y. Shaohorn, *Nat. Nanotechnol.*, 2010, **5**, 531–537.

- 35 G. Che, B. B. Lakshmi, E. R. Fisher and C. R. Martin, *Nature*, 1998, **393**, 346–349.
- 36 D. A. C. Brownson, D. K. Kampouris and C. E. Banks, *J. Power Sources*, 2011, **196**, 4873–4885.
- 37 Z. Niu, H. Dong, B. Zhu, J. Li, H. H. Hng, W. Zhou, X. Chen and S. Xie, *Adv. Mater.*, 2013, **25**, 1058–1064.
- 38 W. Weng, Q. Sun, Y. Zhang, S. He, Q. Wu, J. Deng, X. Fang, G. Guan, J. Ren and H. Peng, *Adv. Mater.*, 2015, **27**, 1363.
- 39 K. Jiang, J. Wang, Q. Li, L. Liu, C. Liu and S. Fan, *Adv. Mater.*, 2011, **23**, 1154–1161.
- 40 K. Liu, Y. Sun, P. Liu, J. Wang, Q. Li, S. Fan and K. Jiang, *Nanotechnology*, 2009, **20**, 335705.
- 41 L. Xiao, Z. Chen, C. Feng, L. Liu, Z.-Q. Bai, Y. Wang, L. Qian, Y. Zhang, Q. Li, K. Jiang and S. Fan, *Nano Lett.*, 2008, **8**, 4539–4545.
- 42 K. Liu, Y. Sun, X. Lin, R. Zhou, J. Wang, S. Fan and K. Jiang, *ACS Nano*, 2010, **4**, 5827–5834.
- 43 S. Luo, K. Wang, J. Wang, K. Jiang, Q. Li and S. Fan, *Adv. Mater.*, 2012, **24**, 2294–2298.
- 44 S. Luo, H. Wu, Y. Wu, K. Jiang, J. Wang and S. Fan, *J. Power Sources*, 2014, **249**, 463–469.
- 45 L. Sun, M. Li, Y. Jiang, W. Kong, K. Jiang, J. Wang and S. Fan, *Nano Lett.*, 2014, **14**, 4044–4049.
- 46 Y. Wu, J. Wang, K. Jiang and S. Fan, *Front. Phys.*, 2014, **9**, 351–369.
- 47 W. Kong, L. Sun, Y. Wu, K. Jiang, Q. Li, J. Wang and S. Fan, *Carbon*, 2016, **96**, 1053–1059.
- 48 X. He, Y. Wu, F. Zhao, J. Wang, K. Jiang and S. Fan, *J. Mater. Chem. A*, 2013, **1**, 11121–11125.
- 49 Y. Yin, C. Liu and S. Fan, *J. Phys. Chem. C*, 2012, **116**, 26185–26189.
- 50 Y. Yu, S. Luo, L. Sun, Y. Wu, K. Jiang, Q. Li, J. Wang and S. Fan, *Nanoscale*, 2015, **7**, 10178–10185.
- 51 Y. Wu, H. Wu, S. Luo, K. Wang, F. Zhao, Y. Wei, P. Liu, K. Jiang, J. Wang and S. Fan, *RSC Adv.*, 2014, **4**, 20010–20016.
- 52 Y. Zhang, W. Y. Bai, X. L. Cheng, J. Ren, W. Weng, P. N. Chen, X. Fang, Z. T. Zhang and H. S. Peng, *Angew. Chem., Int. Ed.*, 2014, **53**, 14564–14568.